Composite Structures 226 (2019) 111285

Contents lists available at ScienceDirect

Composite Structures

journal homepage: www.elsevier.com/locate/compstruct

Sound absorption of micro-perforated sandwich panel with honeycomb-corrugation hybrid core at high temperatures

Yufan Tang[a,b], Fengxian Xin[a,b,*], Tian Jian Lu[c,d]

[a] State Key Laboratory for Strength and Vibration of Mechanical Structures, Xi'an Jiaotong University, Xi'an 710049, PR China
[b] MOE Key Laboratory for Multifunctional Materials and Structures, Xi'an Jiaotong University, Xi'an 710049, PR China
[c] State Key Laboratory for Mechanics and Control of Mechanical Structures, Nanjing University of Aeronautics and Astronautics, Nanjing 210016, PR China
[d] Nanjing Center for Multifunctional Lightweight Materials and Structures (MLMS), Nanjing University of Aeronautics and Astronautics, Nanjing 210016, PR China

ARTICLE INFO

Keywords:
Sandwich panel
Micro-perforation
Sound absorption
High temperature

ABSTRACT

A combined theoretical and numerical study is carried out to evaluate the sound absorption performance of a micro-perforated sandwich panel with perforated honeycomb-corrugation hybrid core (PHCH) at high temperatures up to 700 K. The theoretical model is established based on the classical Maa theory for micro-perforated panels and the method of electro-acoustic analogy. Validity of the model is checked against direct numerical simulations performed on COMSOL Multiphysics. Sound absorption properties of PHCH and its competitors obtained at different temperatures reveal that temperature affects remarkably their low-frequency performance. Average particle velocity in the perforation hole is numerically calculated as a function of temperature, and good agreement between sound absorption peaks and particle velocity peaks is achieved. To further demonstrate the superiority of PHCH in low-frequency sound absorption, the half-absorption bandwidths of PHCH are compared to those of its competitors at high temperatures. The influence of facesheet and corrugation are also studied, illustrating that the former plays a more significant role than the latter. The proposed sandwich structure shows promising engineering applications not only as a load-bearing structure, but also as a sound absorber, even at high temperatures.

1. Introduction

Ultralight sandwich structures have been widely applied in various engineering fields, such as ships [1,2], submarines [3,4], aircrafts [5,6], buildings [7,8] and so on, for great advantages in specific stiffness, specific strength and energy absorption. With particularly tailored core configurations, they can also exhibit huge multi-functionalities in electromagnetic, thermal and acoustic fields. Therefore, in recent years, great efforts have been made by many researchers in the pursuit of innovative sandwich configurations to enhance further the mechanical properties and realize superior multi-functions.

There exist numerous works about the acoustic properties of sandwich structures. For instance, Zhou and Crocker [9] established a theoretical model to predict the sound transmission loss of foam-filled honeycomb sandwich panels and verified the predicted results with experimental measurements. Honeycomb sandwich panel with porous facesheet was studied by Endo and Kim [10] as a direct sound reduction device. Talebitooti and his coauthors developed theoretical models to investigate the sound transmission properties of composite sandwich shells, where the Biot's theory was employed to model the porous materials [11–14]. Similar studies on the sound transmission characteristics of honeycomb sandwich panels filled with and without porous materials can be found in Refs. [15–17]. In addition to sound isolators, sandwich panels with honeycomb cores can be used as sound absorbers as well, for the cavity behind the facesheet serves as the cavity in a Helmholtz resonator if facesheet perforations are introduced as the neck [18]. Subsequently, the absorption performance of micro-perforated metallic sandwich panels with honeycomb core (PH) is investigated [19,20], which can be applied as the liner in airplane turbofan duct [21]. Sakagami and coauthors [22] calculated the absorption coefficient of honeycomb backed micro-perforated panel absorber, finding that the honeycomb wall thickness affects the absorption characteristics, especially the peaks. The absorption performance of sandwich planks consisted of honeycomb grid and foam was investigated by Lin and coauthors [23]. However, the absorption bandwidth of this kind of single-layer sound absorbers is relatively narrow compared to double-layer sound absorbers [24]. Hence, even though a PH possesses good mechanical properties and acoustic properties at the

* Corresponding author.
E-mail addresses: fengxian.xin@gmail.com (F. Xin), tjlu@nuaa.edu.cn (T.J. Lu).

https://doi.org/10.1016/j.compstruct.2019.111285
Received 21 June 2018; Received in revised form 17 June 2019; Accepted 30 July 2019
Available online 31 July 2019
0263-8223/

same time, there is still much room for improvement.

Temperature has always been a critical factor affecting the performance of materials and structures, including sandwich structures. Temperature-dependent mechanical properties of sandwich structures have been extensively studied, such as compression [25,26], buckling [27,28], vibration [29,30] and bending [31,32]. When temperature is high, big drop in sandwich strength or stiffness was observed. Besides mechanical properties, acoustic properties are likewise easily affected by temperature. At the same time, acoustic devices and structures are commonly found high temperature applications. Assaf and coauthors [33] presented a finite element (FE) method to calculate the diffuse sound transmission loss of sandwich plates. They took the frequency-temperature dependence of visco-elastic material properties into account, and made use of an experimentally derived visco-elastic constitutive law. However, although there exist numerous studies on the sound absorption properties of fibrous materials [34–36] and metal foams [37,38] at high temperatures, few studies have looked into the temperature-dependent sound absorption performances of load bearing sandwich structures having micro-perforations. Note that, compared to traditional sound absorbing fibrous materials and foams, micro-perforated sandwich structures can not only absorb sound but also carry structural load.

Recently, we proposed a sandwich structure with honeycomb-corrugation hybrid core [39,40] and demonstrated its great advantage in energy absorption and compressive strength over traditional structures, like honeycomb- and corrugated-core sandwiches. Subsequently, we also found that, upon introducing micro-perforations (submillimeter in diameter) on its facesheet and corrugation, a sandwich panel with perforated honeycomb-corrugation hybrid (PHCH) core is formed, showing great low-frequency sound absorption potential [41]. This innovative sandwich structure is ultralight and exhibits not only great mechanical properties (e.g., stiffness, strength and energy absorption) but also superior sound absorption, ideal for multifunctional applications.

Although the effects of high temperature on the mechanical properties and sound transmission characteristics of sandwich structures have been extensively explored, the dependence of sound absorption on temperature receives much less attention. In this paper, a temperature-dependent theoretical model for the acoustic impedance under normal incidence is established for micro-perforated sandwich panel with PHCH core. A clear relationship between the temperature and the acoustic impedance is established. Subsequently, the sound absorption curves and acoustic impedance characteristics of the proposed sandwich structure are calculated using the model and compared with those of micro-perforated sandwich panel with honeycomb-corrugation hybrid core (HCH) as well as those of micro-perforated sandwich panel with honeycomb core (PH). It is demonstrated that the PHCH exhibits wider absorption bandwidths and better low-frequency behaviors at high temperatures. Finally, discussions about the temperature effects on sound absorption are made along with variations of facesheet thickness and corrugation plate thickness.

2. Theoretical model and numerical method

With reference to Fig. 1(a), the micro-perforated all-metallic sandwich panel with PHCH core is composed of a micro-perforated top facesheet, a micro-perforated corrugation, honeycomb insertions, and a (non-perforated) bottom facesheet. The honeycomb insertions are cut into trapezoidal shape before being precisely fitted to the corrugation, forming thus the PHCH core. The inner side length and outer side length of the honeycomb insertions are b_2 and b_1, as shown in Fig. 1(b), which is a half section view of one unit cell in the PHCH. The facesheet and corrugation have thickness t_f and t_c, respectively, and the PHCH core has height D. In the absence of perforations, a sandwich panel with honeycomb-corrugation hybrid core is a super mechanical structure [39,40] but absorbs little sound. Once sub-millimeter perforations are introduced to the upper facesheet and the corrugation, however, the whole structure acquires remarkable sound absorption capability while the mechanical properties of the structure are only slightly affected by these micro-perforations. This is because a single micro-perforation and the cavity behind it constitute a Helmholtz resonator, dissipating thus the acoustic energy via the viscous boundary layer at the perforation hole especially at its natural frequency. To facilitate theoretical modeling, the perforation hole is assumed to be circular and located at the center of each honeycomb cell. Throughout the current study, square honeycombs are considered. The perforation diameter is represented by $d_{n,l}$ with n and l denoting the honeycomb cell number and the layer number, respectively. Correspondingly, the diameters on the upper facesheet are $d_{1,1}$, $d_{2,1}$, … $d_{6,1}$, while those on the corrugation are $d_{2,2}$, $d_{3,2}$, $d_{5,2}$ and $d_{6,2}$, as shown in Fig. 1(b).

Consider a plane sound wave p_i normally propagating towards the surface of the PHCH-cored sandwich panel. Part of the incident acoustic energy is absorbed. The ratio of the absorbed energy to the incident energy is defined as the sound absorption coefficient, calculated by [42]

$$\alpha = 1 - \left|\frac{Z_s - Z_0}{Z_s + Z_0}\right|^2 \tag{1}$$

in which Z_s is the surface impedance of the PHCH-cored sandwich panel and $Z_0 = \rho_0 c_0$ is the characteristic impedance of air, ρ_0 and c_0 being the mass density of and sound speed in air, respectively. The surface impedance can be normalized as $z_s = Z_s/\rho_0 c_0$ and hence the relationship between specific surface impedance and sound absorption coefficient is:

$$\alpha = 1 - \left|\frac{\mathrm{Re}(z_s) - 1 + j\cdot\mathrm{Im}(z_s)}{\mathrm{Re}(z_s) + j\cdot\mathrm{Im}(z_s) + 1}\right|^2 \tag{2}$$

In the equation above, j refers to the imaginary unit. Re and Im mean the real part and the imaginary part. The sound absorption coefficient is seen to achieve its maximum only when the real part of specific surface impedance equals to 1 and the imaginary part equals to 0.

The surface impedance of the PHCH sandwich can be obtained by adopting the electro-acoustic analogy method, which is based on the series-parallel connection demonstration [24,43], as:

$$\begin{cases} Z_s = \frac{6b_1^2}{b_2^2}\left(\sum_{n=1}^{6}\frac{1}{Z_{n,1}}\right)^{-1} \\ Z_{n,l} = Z_{Mn,l} + Z_{Cn,l} \end{cases} \tag{3}$$

The total surface impedance is closely related to the impedance of each honeycomb block in the first layer, $Z_{n,1}$, which can be obtained after determining $Z_{Mn,l}$ and $Z_{Cn,l}$. The impedance of the cavity with rigid back, $Z_{Cn,l}$, is given by Brekhovskikh [44] as:

$$\begin{cases} Z_{Cn,1} = Z_0\frac{Z_{n,2}\cos(kD_{n,1}) + jZ_0\sin(kD_{n,1})}{Z_0\cos(kD_{n,1}) + jZ_{n,2}\sin(kD_{n,1})}, \quad n = 2, 3, 5, 6 \\ Z_{Cn,l} = -jZ_0\cot(kD_{n,l}), \quad n \neq 2, 3, 5, 6 \text{ and } l \neq 1 \end{cases} \tag{4}$$

here $k = \omega/c_0$ refers to the wavenumber, and ω denotes the angular frequency of incident sound wave. The impedance of the micro-perforated panel $Z_{Mn,l}$ is dominated by the perforations on it, which may be visualized as small circular tubes. Because of the existence of viscous and inertia forces, the fluid in each tube may be approximated as coaxial cylindrical layers moving parallel to each other. With the sound pressure difference between the two ends of the tube denoted by Δp, the equation of fluid motion is [45]:

$$\rho_0\ddot{u} - \frac{\eta}{r}\frac{\partial}{\partial r}\left(r\frac{\partial}{\partial r}u\right) = \frac{\Delta p}{t} \tag{5}$$

where η is the dynamic viscosity of air, and u, r and t refer to the axial particle velocity, the radius vector, and the tube length, respectively. The solution for Eq. (5) is [45]:

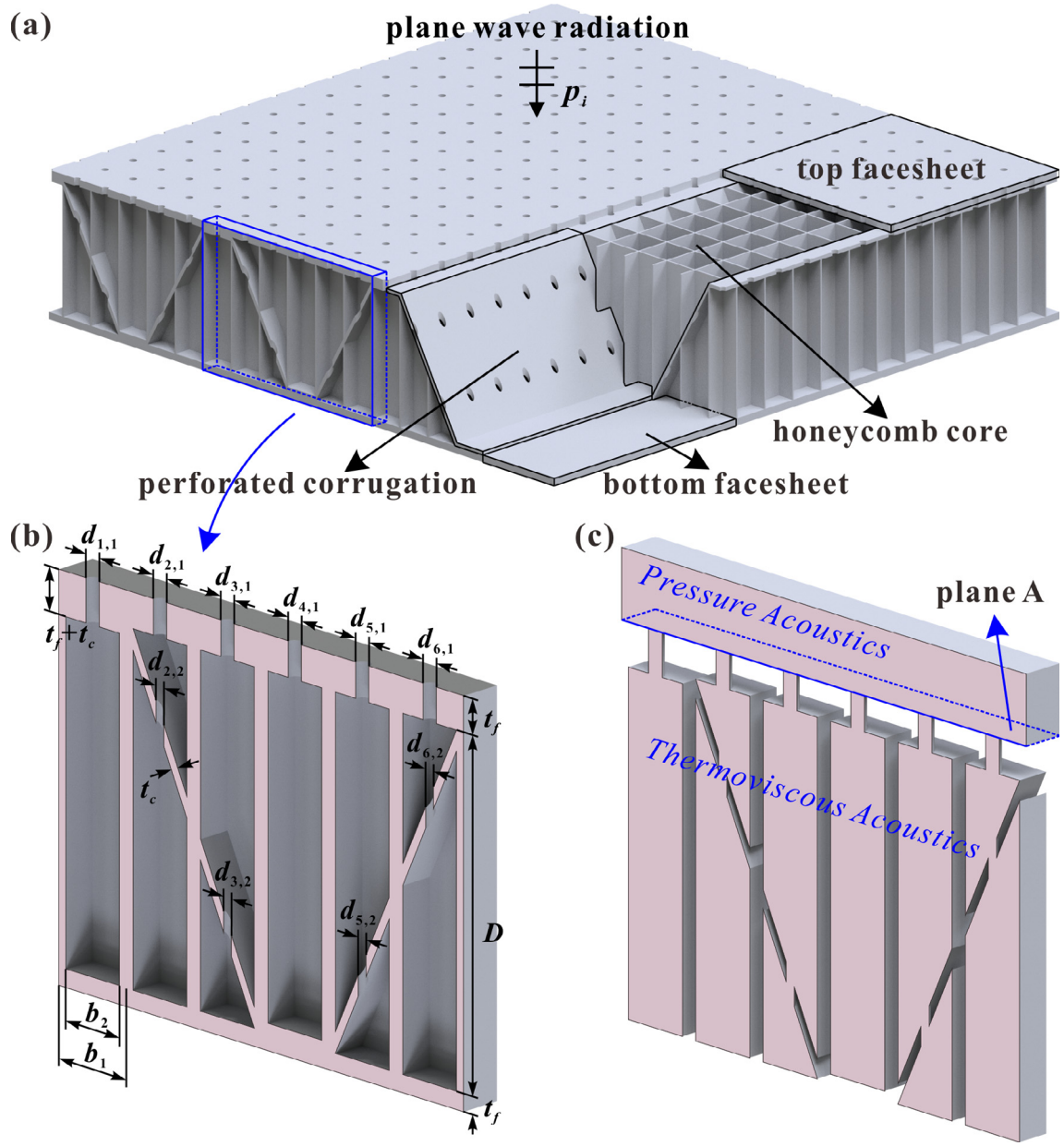

Fig. 1. (a) Schematic illustration of PHCH; (b) Half section view of one unit cell in PHCH; (c) Half section view of the numerical model for PHCH.

$$u(r) = -j\frac{\Delta p}{\omega\rho_0 t}\left[1 - \frac{B_0\left(\sqrt{-j\frac{\omega\rho_0}{\eta}}r\right)}{B_0\left(\sqrt{-j\frac{\omega\rho_0}{\eta}}r_0\right)}\right] \tag{6}$$

Here, r_0 is the tube radius, and B_n is Bessel's function of the first kind and n-th order. Physically, as the acoustic impedance of the tube is the ratio of acoustic pressure difference to average velocity, it can be deduced as:

$$Z = \frac{\Delta p}{\bar{u}} = j\omega\rho t\left[1 - \frac{2}{\sqrt{-j\frac{\omega\rho_0}{\eta}}}\frac{B_1\left(\sqrt{-j\frac{\omega\rho_0}{\eta}}r_0\right)}{B_0\left(\sqrt{-j\frac{\omega\rho_0}{\eta}}r_0\right)}\right]^{-1} \tag{7}$$

where $\bar{u}$ is the averaged velocity inside the tube.

Eq. (7) is further arranged by Maa in a simpler form without the Bessel function [46], as:

$$Z = \frac{32\eta t_{n,l}}{d_{n,l}^2}\left(1 + \frac{\omega\rho_0 d_{n,l}^2}{128\eta}\right)^{0.5} + j\omega\rho_0 t_{n,l}\left[1 + \left(9 + \frac{\omega\rho_0 d_{n,l}^2}{8\eta}\right)^{-0.5}\right] + E_c \tag{8}$$

This form is more precise, because the last term E_c is introduced as the end correction for relatively large circular perforations on a thin panel:

$$E_c = \frac{\sqrt{2\omega\rho_0\eta}}{2} + 0.85j\omega\rho_0 d_{n,l} \tag{9}$$

Eq. (8) characterizes the impedance of a single perforation hole. To obtain the impedance of the whole micro-perforated panel, the porosity of the perforation (i.e., perforation ratio) should be considered. The impedance of the micro-perforated panel, $Z_{Mn,l}$, can be given as a function of the impedance for the tube Z and the porosity $p_{n,l}$, as:

$$Z_{Mn,l} = \frac{Z}{p_{n,l}} \tag{10}$$

Table 1
The values of C_N.

C_N	Values
C_0	-8.38278×10^{-7} Pa·s
C_1	$8.35717342 \times 10^{-8}$ Pa·s·K^{-1}
C_2	$-7.69429583 \times 10^{-11}$ Pa·s·K^{-2}
C_3	$4.6437266 \times 10^{-14}$ Pa·s·K^{-3}
C_4	$-1.06585607 \times 10^{-11}$ Pa·s·K^{-4}

In the above equations, ($d_{n,l}$, $t_{n,l}$, $p_{n,l}$, $D_{n,l}$) denote separately the perforation diameter, the perforation depth, the porosity, and the cavity depth of the n-th honeycomb block in the l-th layer. For the first layer, the perforation depth is just the facesheet thickness, because the small circular holes are perforated vertically to the facesheet. For the second layer, the perforation depth is defined as t_c in the current study. The porosity means the proportion of the perforation area over the whole panel area. The cavity depth refers to the distance from the center of the perforation to the panel. With reference to Fig. 1(b), it is worth noting that the first and the forth honeycomb blocks only have one layer, while the others have two layers. So the proposed sandwich structure is a hybrid sound absorber, which is a combination of single-layer sound absorbers and double-layer sound absorbers, thus helpful for broadening the absorption bandwidth.

In order to validate the above theoretical model, a finite element model is further proposed. Numerical simulations are performed with COMSOL Multiphysics, using the module of the Acoustic-Thermoacoustic Interaction on the basis of Thermo-viscous Acoustics and Pressure Acoustics. The equations for Thermo-viscous Acoustics are as follows:

$$\begin{aligned} &j\omega\rho + \rho_0\nabla\cdot\mathbf{u} = 0 \\ &j\omega\rho_0\mathbf{u} - \nabla\cdot\left\{-p\mathbf{I} + \eta\left[\nabla\mathbf{u} + (\nabla\mathbf{u})^{\mathrm{T}} - \left(\tfrac{2}{3}\eta - \eta_B\right)(\nabla\cdot\mathbf{u})\mathbf{I}\right]\right\} = 0 \\ &j\omega\rho_0 C_p T - j\omega\alpha_0 T_0 p - \nabla\cdot(\kappa\nabla T) = 0 \end{aligned} \tag{11}$$

where ρ, T and p refer to the variations of air density, temperature and air pressure; $\boldsymbol{u}$ and $\boldsymbol{I}$ are the vibration velocity of the particle and the identity matrix, and $()^{\mathrm{T}}$ denote the transposition of a matrix; η_B, C_p, α_0 and κ are separately the bulk viscosity, specific heat at constant pressure, thermal expansion coefficient and thermal conductivity of air.

The equation for Pressure Acoustics is as follows:

$$\nabla\cdot\left[-\frac{1}{\rho}(\nabla p - \mathbf{q}_d)\right] - \frac{\omega^2 p}{\rho c_0^2} = Q_m \tag{12}$$

where $\mathbf{q}_d$ and Q_m are the dipole domain source and the monopole domain source. In this study, they are equal to 0.

The numerical model is displayed in Fig. 1(c). Plane A is a demarcation boundary, below which the model simulates the air in PHCH using Thermoviscous Acoustics, while up which the incident acoustic wave region is modeled by Pressure Acoustics. Sound hard boundary is applied on all the surfaces below plane A, so as to imitate the rigid assumption of the sandwich structure. Periodic condition is employed for the upper part of the model to realize periodic arrangements in the transverse direction. Given an acoustic wave incidence, the acoustic pressure p and the particle velocity of air v_z can be numerically calculated, and hence the specific acoustic impedance can be obtained as [41]:

$$z_s = \frac{\langle p\rangle_{\mathrm{A}}}{\langle v_z\rangle_{\mathrm{A}}}\cdot\frac{1}{Z_0} \tag{13}$$

in which $\langle\cdot\rangle_{\mathrm{A}}$ represents the area-averaging manipulation over plane A. Once the specific acoustic impedance is known, the sound absorption can be calculated by using Eq. (2).

3. Temperature dependent variables of air

The sound absorption performance of the present micro-perforated sandwich structure is greatly influenced by the temperature dependent variables of air, including: dynamic viscosity η, sound speed c_0 and mass density ρ_0. The dynamic viscosity of a fluid expresses its resistance to shearing flow, where adjacent layers move parallel to each other with different speeds. The dynamic viscosity contributes to the shear stress τ by:

$$\tau = \eta\frac{\partial u}{\partial y} \tag{14}$$

where $\partial u/\partial y$ is the shear velocity gradient along the y-direction. So the dynamic viscosity signifies the ratio of shear stress within the flow to velocity gradient. By changing both the dynamic viscosity and the velocity distribution of air in the structure, the temperature influences the acoustic impedance characteristic of the structure.

The dynamic viscosity of air in COMSOL Multiphysics is given in a numerical form, as:

$$\eta_C = \sum_{N=0}^{4} C_N\cdot T_0^N \tag{15}$$

where T_0 is the temperature and C_N are constant coefficients listed in Table 1.

In addition, the dynamic viscosity of air has been given by Smits [47] in a theoretical form, as:

$$\eta_S = \eta_{init}\cdot\frac{T_{init} + C_S}{T_0 + C_S}\cdot\left(\frac{T_0}{T_{init}}\right)^{1.5} \tag{16}$$

in which $\eta_{init} = 1.827 \times 10^{-5}$ Pa·s, $T_{init} = 291.15$ K and $C_S = 120$ K.

As dynamic viscosity is a vital property of air both in theoretical modeling and numerical simulation, it is necessary to make a comparison between the two formulas of (15) and (16). Fig. 2 plots the dynamics viscosity as a function of temperature, showing that the dynamic viscosity changes remarkably with the temperature. The difference between the results predicted with the two formulas is quite small, no more than 3% at any discussed temperature. It is seen from Fig. 2 that the dynamic viscosity almost doubles from 300 K to 700 K, which will then pronouncedly alter the corresponding velocity distribution for a given pressure gradient. Therefore, the surface impedance, which is closely related to velocity and pressure fields, also varies significantly with the temperature. As a result, an obvious peak shift will be observed for the sound absorption curve, as shown below.

Another important variable is the viscous boundary layer thickness, given as:

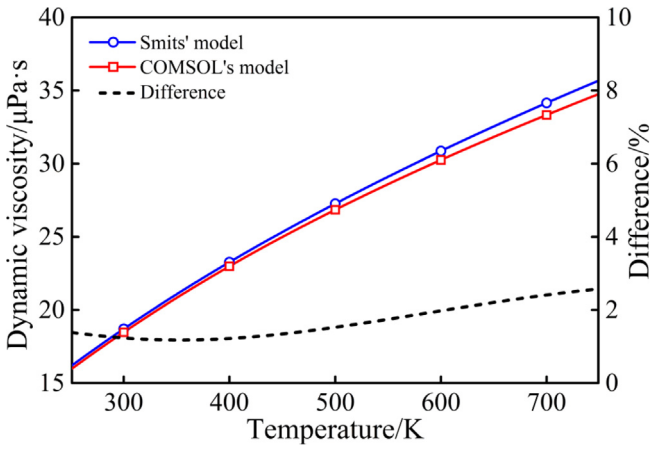

Fig. 2. Dynamic viscosity plotted as a function of temperature: comparison between Smits' model and COMSOL Multiphysics.

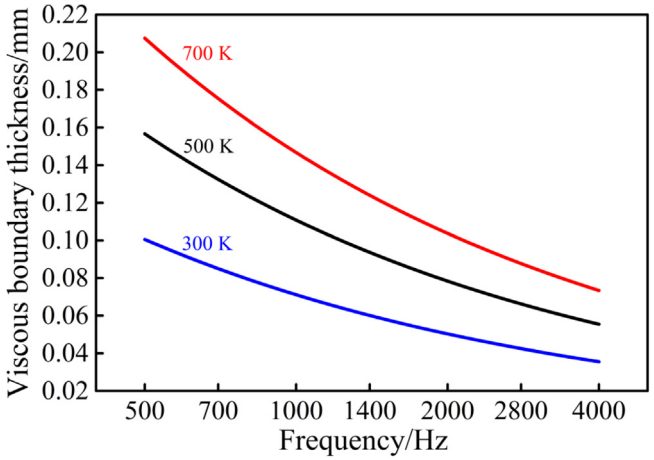

Fig. 3. Viscous boundary layer thickness plotted as a function of frequency for selected temperatures.

$$d_{th} = \sqrt{\frac{2\eta}{\omega\rho_0}} \tag{17}$$

The viscous boundary layer is defined here as the layer from the perforation wall to the point at which the viscous flow velocity is 99% of freestream velocity. Fig. 3 plots the viscous boundary layer thickness as a function of frequency at 300 K, 500 K and 700 K. The viscous boundary layer thickness decreases with increasing frequency, but increases with increasing temperature. These variation trends are consistent with Eq. (17). The equation shows a direct relation between the viscous boundary layer thickness and the frequency, while it presents an indirect relation between the viscous boundary layer thickness and the temperature. The viscous boundary layer thickness is proportional to the square root of the dynamic viscosity. Given the positive correlation between dynamic viscosity and temperature, it can be seen that the viscous boundary layer will be thicker if the temperature rises.

Temperature also affects the characteristic impedance of air. Analytically, the dependence of sound speed on temperature is expressed as:

$$c_0 = \sqrt{\gamma R_s T_0} \tag{18}$$

where γ is the heat capacity ratio (1.4 for air) and $R_s = R/M$ is the specific gas constant. $R = 8.314\ \mathrm{J{\cdot}mol^{-1}{\cdot}K^{-1}}$ and $M = 0.029\ \mathrm{kg{\cdot}mol^{-1}}$ are the molar gas constant and molar mass of air, respectively.

Finally, the mass density of air varies with temperature as:

$$\rho_0 = \frac{P_0 M}{R T_0} \tag{19}$$

in which $P_0 = 101.325$ kPa is the atmosphere pressure.

4. Results and discussions

The proposed theoretical model is validated by numerical simulations in terms of sound absorption curves and specific impedance curves for sandwich panels. Table 2 lists relevant geometrical parameters. Two groups are separated by different cavity thickness D. Sample A, B and C are used to evaluate the sound absorption performances of micro-perforated sandwich panels with PHCH core, HCH (honeycomb-corrugation hybrid) core and PH (perforated honeycomb) core. Samples D, E and F are the optimized candidates to compare the sound absorption potential between PHCH and its competitors. The unit cells of PHCH, HCH and PH are shown in Fig. 4. With identical top and bottom facesheets, the three sandwich structures differ only in their cores. PHCH has perforations on the corrugation [see Fig. 4(a)], while there is no perforation in any part of HCH [see Fig. 4(b)]. PH is only made of honeycomb, as shown in Fig. 4(c).

4.1. Absorption curve and impedance

Fig. 5 plots the sound absorption versus frequency curves of PHCH at 300 K, 500 K and 700 K. All the parameters are the same as those of Sample A in Table 2. The theoretical model predictions approach well to the numerical simulation results at all temperatures. The absorption peak moves to higher frequencies when the temperature rises. At the same time, the peak value of the absorption curve diminishes.

To clearly understand the reason for the sound absorption peak shifting, the Helmholtz resonance theory can be applied, which can predict the relationship between dimensional parameters and the peak frequency [48]. Actually, the perforation hole in the cover and its backed cavity constitute one Helmholtz resonator, which is just like one mass-spring system. The air in the perforation hole behaves as the mass, while the air in the backed cavity behaves as the spring. When sound wave incidents, this “mass-spring system” works, namely, the air in the perforation hole vibrates as a whole mass and the air in the backed cavity provides the spring restoring force. The friction between the air and the perforation wall can consume the sound energy to heat energy, resulting in the sound absorption performance of the Helmholtz resonator. At the resonance frequency of the “mass-spring system”, the strongest vibration of the air in the perforation hole corresponds to the strongest friction and the sound absorption peak. According to the Helmholtz resonance theory, for the Helmholtz resonator, the “mass” is $m = \rho_0 lS$ and the “stiffness of the spring” is $k = \rho_0 c_0^2 S^2/V$, thus the sound absorption peak frequency (i.e., the resonance frequency) is

$$\omega_r = \sqrt{\frac{k}{m}} = \sqrt{\frac{c_0^2 S}{Vl}} \tag{20}$$

where ρ_0 is air density, c_0 is sound speed, l and S refer to the length and cross-sectional area of perforation hole, respectively, V denotes the volume of the backed cavity. As above mentioned, the elevated temperature mainly affects the viscosity, sound speed and density of the air, while the sound absorption peak frequency is mainly affected by the sound speed when the temperature rises [Eq. (20)]. With the increase of the temperature, the sound speed in air increases, which induces the increase of the “stiffness of the spring”, eventually resulting in the increase of the sound absorption peak frequency.

In one word, high temperature partly destroys the low-frequency absorption performance of PHCH. As a result, it is more difficult and meaningful to realize good sound absorption at low frequencies than that at high frequencies. As a result, in subsequent sections, this study

Table 2
Geometrical parameters of PHCH, HCH and PH.

Geometrical dimensions	d_{11}	d_{21}	d_{31}	d_{41}	d_{51}	d_{61}	d_{22}	d_{32}	d_{52}	d_{62}	t_f	t_c	b_1	b_2	D
Sample A	0.4	0.4	0.5	0.5	0.6	0.6	0.2	0.2	0.3	0.3	0.5	0.2	4	3.8	24
Sample B	0.4	0.4	0.5	0.5	0.6	0.6	/	/	/	/	0.5	0.2	4	3.8	24
Sample C	0.4	0.4	0.5	0.5	0.6	0.6	/	/	/	/	0.5	/	4	3.8	24
Sample D	0.43	0.74	0.99	0.33	0.99	0.34	0.33	0.29	0.3	0.51	0.24	0.33	3.3	3	40
Sample E	0.5	0.55	0.56	0.48	0.82	0.54	/	/	/	/	0.75	0.2	3.2	2.9	40
Sample F	0.25	0.24	0.24	0.24	0.23	0.25	/	/	/	/	0.2	/	2	1.7	40

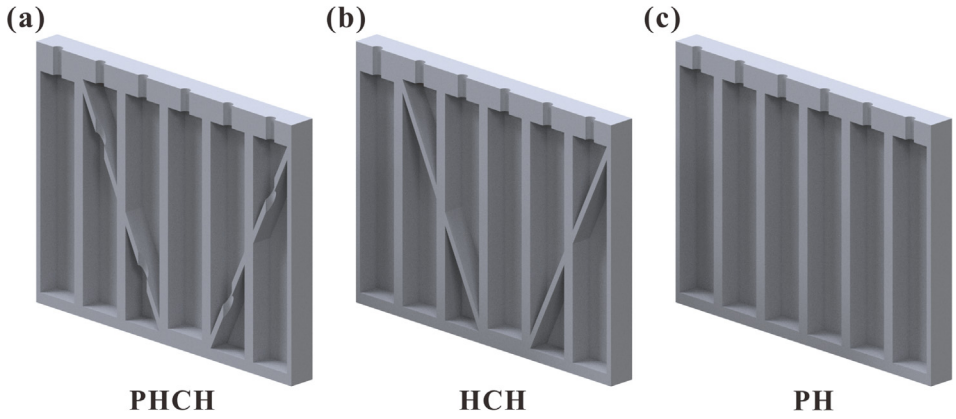

Fig. 4. Half-sectional view of unit cell for (a) PHCH; (b) HCH; (c) PH.

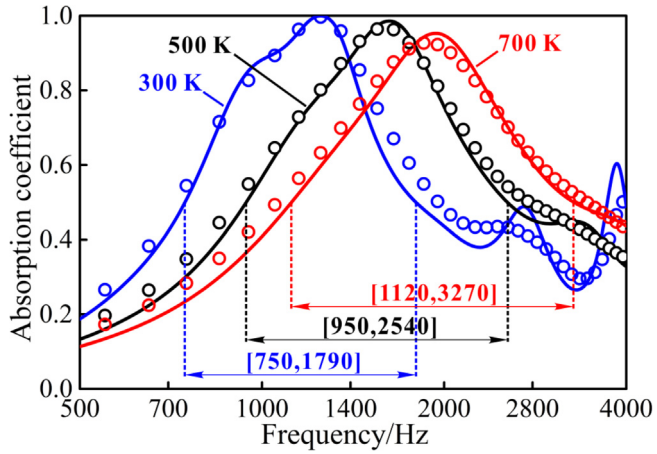

Fig. 5. Sound absorption curves of PHCH-cored sandwich panel at different temperatures. The solid lines refer to theoretical results and the circles are numerical results.

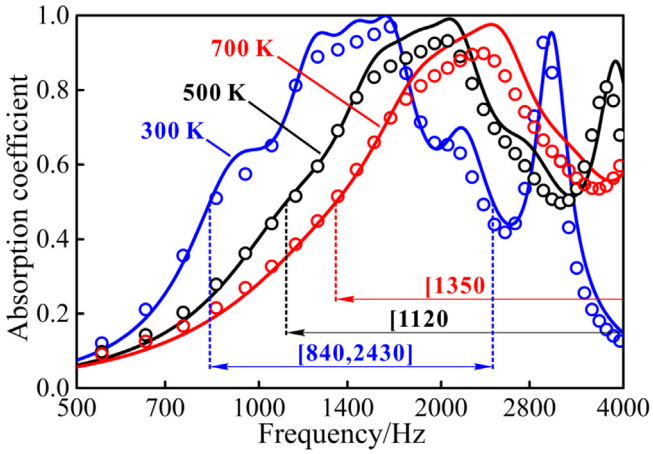

Fig. 7. Sound absorption curves of HCH-cored sandwich panel at different temperatures. The solid lines refer to theoretical results and the circles represent numerical results.

focuses on the temperature effect on low-frequency (below 4000 Hz) absorption. Half-absorption bandwidth refers to the frequency band where sound absorption coefficients are larger than 0.5. Based on the theoretical results, the half-absorption bandwidths for PHCH at 300 K, 500 K and 700 K are 1040 Hz, 1590 Hz and 2150 Hz, respectively, which exhibit a remarkable enlarging tendency. However, low-frequency sound attenuation is always more difficult to achieve. This is because the frequency of absorption peak is roughly in inverse

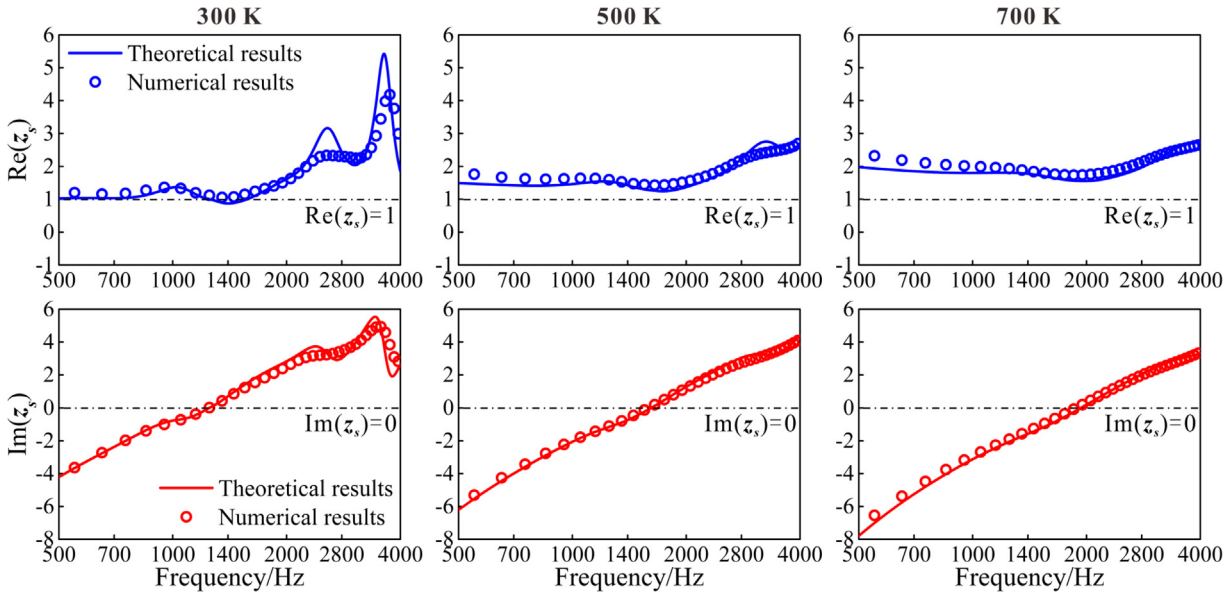

Fig. 6. Specific surface impedance (real part and imaginary part) of PHCH at different temperatures.

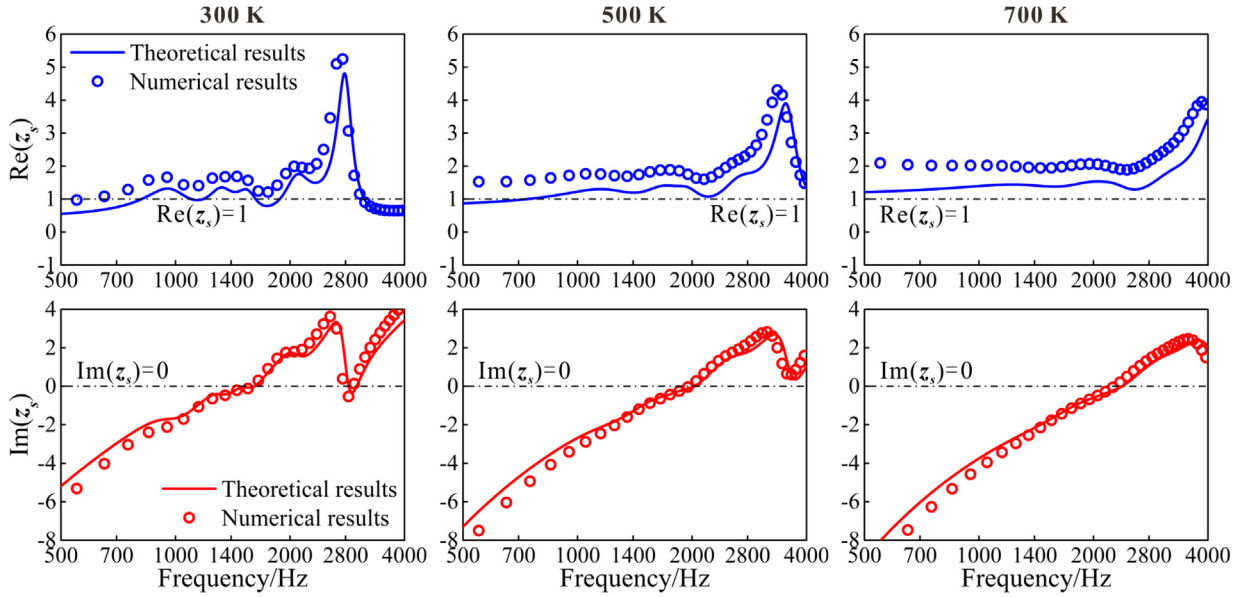

Fig. 8. Specific impedance (real part and imaginary part) of HCH at different temperatures.

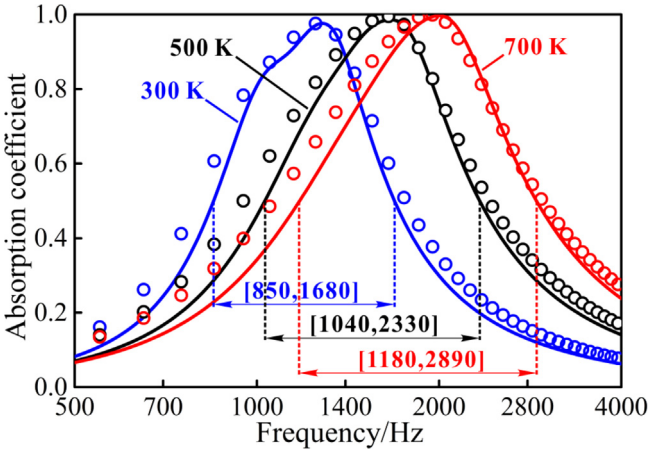

Fig. 9. Sound absorption coefficient of PH-cored sandwich panel at different temperatures. The solid lines refer to theoretical results and the circles refer to numerical results.

proportion to the cavity [48], so more weight and cost will be needed to absorb low-frequency noise. There are many methods to take this thought into consideration. One simple way is to use the concept of octave, which can be calculated as:

$$B_o = \log_2 \frac{f_1}{f_2} \tag{21}$$

in which f_1 and f_2 denote two threshold frequencies where sound absorption coefficient is exactly 0.5. In this way, it is found that the half-absorption bandwidths for PHCH at 300 K, 500 K and 700 K are 1.255 octaves, 1.419 octaves and 1.546 octaves. The higher the surrounding temperature is, the wider the half-absorption band will be. Benefiting from the wider half-absorption bandwidth, the average sound absorption coefficient of PHCH at 700 K is 0.59, larger than 0.56 at 500 K and 0.51 at 300 K.

It is worth noting that the absorption curve tends to be more flattened if the temperature is increased. Less extremums and smaller extreme values appear after the first peak. This is directly reflected by the specific surface impedance of PHCH, as shown in Fig. 6. The real part and the imaginary part are both having less and smaller peaks as the temperature becomes higher. According to Eq. (2), perfect absorption ($\alpha = 1$) requires the real part being 1 and the imaginary part being 0. Meanwhile, the closer the real part approaches to 1 and the imaginary part approaches to 0, the better absorption performance PHCH will have. From the upper three figures of Fig. 6, we can see that the real part of specific surface impedance will be getting farther and farther away from 1 if the temperature is raised. So it will be more and more difficult to satisfy the condition of perfect absorption. As a result, the peak values of the absorption curve drop. The lower three figures show that the imaginary part of specific impedance is moving from low frequencies to high frequencies with the temperature rising. Thus the intersection of the impedance line and the zero point moves to higher frequencies. Consequently, the peak frequency of the absorption curve turns out to be higher.

For comparison, the absorption performance of HCH-cored sandwich panel is also investigated and presented in Fig. 7, using the same parameters as Sample B in Table 2. Note that, in Table 2, the perforation diameter on the corrugation is empty, meaning that there are no perforations on the corrugation. It is seen from Fig. 7 that the numerical results agree well with the theoretical ones. When the temperature is raised, the results of Fig. 7 reveal that the same conclusions for PHCH also apply for HCH: absorption peak moving to higher frequency, peak value dropping down, and gentler variation of the absorption curve.

One thing we can see from Fig. 7 that is apparently different from the results in Fig. 5 is that, around the frequencies where the first absorption peaks happen, the numerical results are slightly smaller than the theoretical predictions. This is because the numerical results for the real part of the specific impedance are generally bigger than the corresponding theoretical predictions, as shown in Fig. 8. In contrast, the imaginary part curves have relatively larger slopes. Hence the imaginary part mainly decides the frequency for the absorption peak. However, once the imaginary part fulfills or almost satisfies the demand for perfect absorption, the real part becomes the key variable. When the theoretical curve of the real part passes through $\mathrm{Re}(z_s) = 1$ at around 1600 Hz, taking the curve at 300 K for example, the numerical results does not reach to 1. Consequently, around the peak frequencies, the theoretical absorption coefficients are slightly larger than the numerical results. In addition, the present results demonstrate that the bandwidths at 500 K and 700 K are much bigger than that at 300 K. This is because the first troughs of the absorption curves at 500 K and 700 K are both larger than 0.5, so the bandwidths are not intercepted before the troughs. For simplicity, the threshold frequencies are not presented within the range in this study.

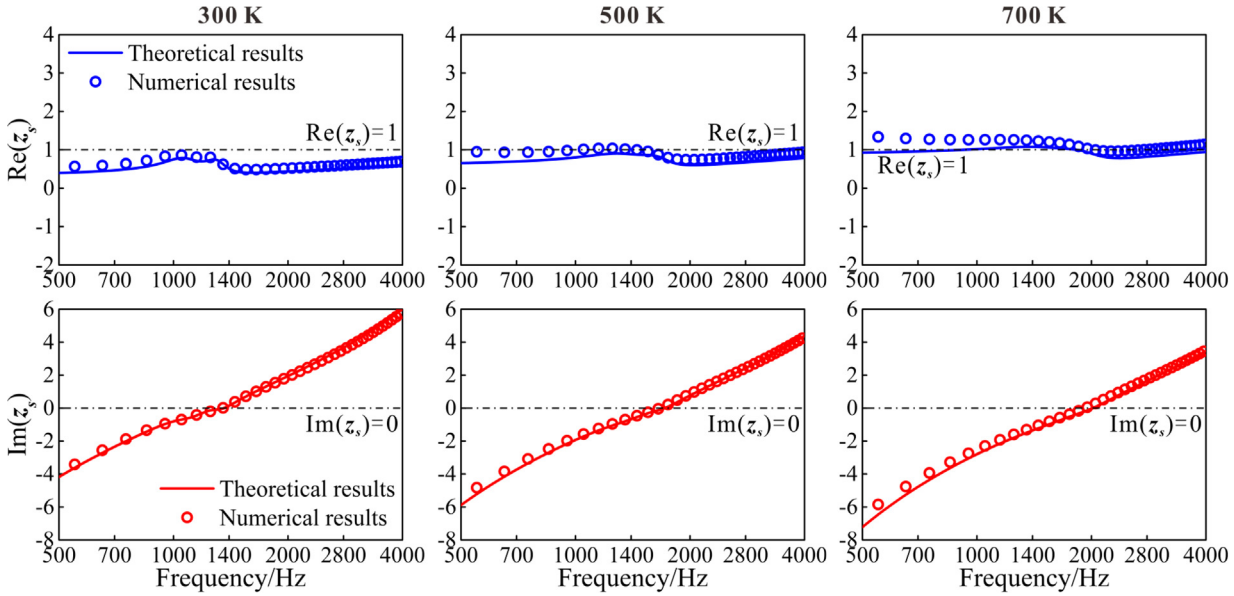

Fig. 10. Specific impedance (real part and imaginary part) of pH at different temperatures.

Fig. 9 displays the variation of sound absorption with temperature for PH-cored sandwich panel. All the parameters are the same as Sample C in Table 2. When the temperature rises, the absorption peak value increases, which is different from that of PHCH. This particular variation is the consequence of the relationship between the real part of specific impedance and the temperature, as shown in Fig. 10. The real part curves are nearly parallel to $\mathrm{Re}(z_s) = 1$ and also very close to $\mathrm{Re}(z_s) = 1$. When the imaginary part satisfies $\mathrm{Im}(z_s) = 0$, the peak of the absorption curve appears. At this moment, the real part determines the value of the peak. At 300 K, the real part curve is obviously lower than $\mathrm{Re}(z_s) = 1$, thus the peak value of the absorption curve is unable to reach 1. With the temperature rising, the real part curve gradually approaches to $\mathrm{Re}(z_s) = 1$, enlarging the peak value of the absorption curve. In fact, PHCH and PH have the same variation trends of the real part of the specific impedance curves with temperature. The only difference is that the real part for PH changes from below 1 to greater than 1 as the temperature is increased, while that of PHCH is larger than 1 all the time. The half-absorption bandwidths of pH at 300 K, 500 K and 700 K are 0.983 octaves, 1.164 octaves and 1.292 octaves, respectively. So, the same as PHCH, the half-absorption band broadens with increasing temperature. However, the bandwidth of pH is apparently narrower than that of PHCH.

In summary, from the absorption curves of PHCH, HCH and PH presented above, it is seen that PHCH has the lowest initial frequency of the half-absorption band under the same circumstances. That is, PHCH has advantages in low-frequency sound absorption over other competitive structures.

4.2. Average particle velocity

The average particle velocity is evaluated here since it closely related to the sound absorption performance. Sound wave propagates by the vibration of particles in the transmission medium. When the frequency of the incident sound wave approaches the resonant frequency, the particles in the neck of Helmholtz resonators oscillate severely, causing great energy dissipation due to internal viscous friction and heat conduction of the medium. The viscous friction and the heat conduction refer separately to viscous energy dissipation and thermal energy dissipation. In the current study, the necks of Helmholtz resonators are the perforation areas in PHCH, HCH and PH. For each type of sandwich structure, Fig. 11 shows the average velocity in the neck at different temperatures calculated by numerical simulations. The extremums in the three figures correspond to the sound absorption peaks in Fig. 5 for PHCH, Fig. 7 for HCH and Fig. 9 for PH. Even the second peaks of the average velocity for HCH at 300 K and 500 K agree well with the absorption curves.

4.3. Optimization

To further demonstrate the superiority of PHCH in sound absorption at high temperatures, comparison among PHCH-, HCH– and PH-cored sandwich panels is made in this section. Optimizations are performed separately for PHCH and its competitors having the same total thickness to fully realize their sound absorption potentials. The optimization process is established to search for the largest average sound absorption coefficient over the selected frequency band (i.e., the objective function). Instead of logarithmic average, linear average is adopted in this study, with simulated annealing selected as the optimization algorithm [49]. To guarantee the effectiveness and comparability of the optimization results, all the elements in the optimization process are kept the same. With regard to the geometrical dimensions, only the total thickness is restricted so as to discuss the sound absorption performance of the three different structures when they occupy the same space.

Table 3 displays the required elements for optimization. L, β, T_i and T_f refer to the Markov chain length, the cooling factor, the initial temperature for annealing and the final temperature for annealing. High initial temperature ensures the ability to jump out of the local optimum at the beginning, and low final temperature guarantees the capability for staying at the global optimum in the end.

Fig. 12 reveals the convergence of the optimization process when using the elements of Table 3. The figure shows the variation tendency as well as the cooling temperature as the iteration cycle proceeds. At first, the average absorption curve fluctuates severely when the cooling temperature is high, because there is a great probability of continually accepting weaker average absorption coefficients at this moment. With the cooling temperature getting lower, the average absorption coefficient tends to become stable, showing that accepting the configuration of the structure with weaker absorption performance becomes harder. At the same time, the average absorption coefficient approaches its global optimum, resulting in less improvement. More importantly, this figure demonstrates the effectiveness of the elements selected in Table 3. Eventually, the average absorption coefficient falls into a small region which may include the global optimum, then exporting a value which is the maximum throughout the whole optimization process.

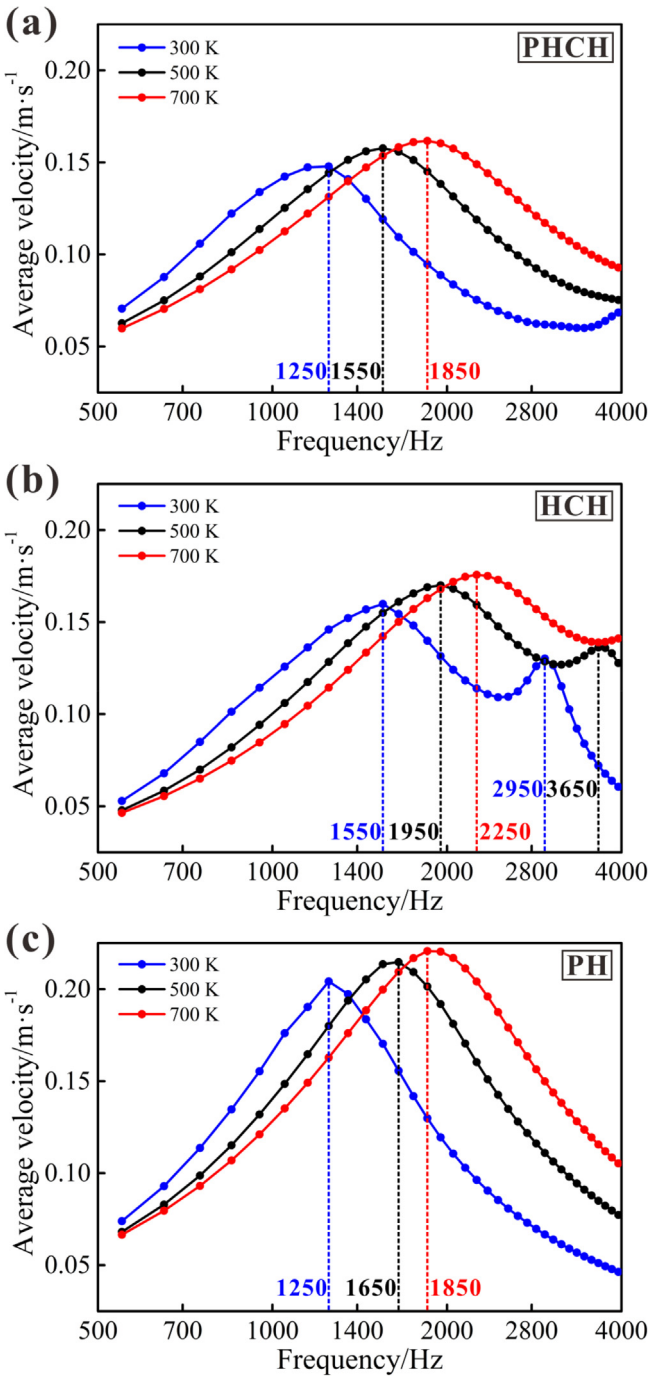

Fig. 11. Average particle velocity in the perforation area on the facesheet of (a) PHCH; (b) HCH; (c) PH.

Table 3
Required elements in the optimization process with simulated annealing.

L	β	T_i	T_f
100	0.99	1000	0.01

Figs. 13–15 display the absorption curves of optimized PHCH, HCH and PH from 500 Hz to 4000 Hz at the temperature of 700 K. All the parameters are the same as those of Sample D, Sample E and Sample F in Table 2. The optimization algorithm is performed using the theoretical method, and the numerical results are presented to validate the theoretical predictions. On the one hand, the initial frequencies of the

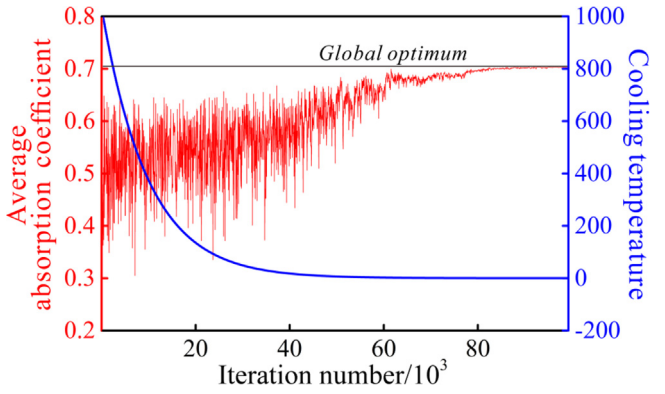

Fig. 12. Variation of cooling temperature and average sound absorption coefficient with iteration number.

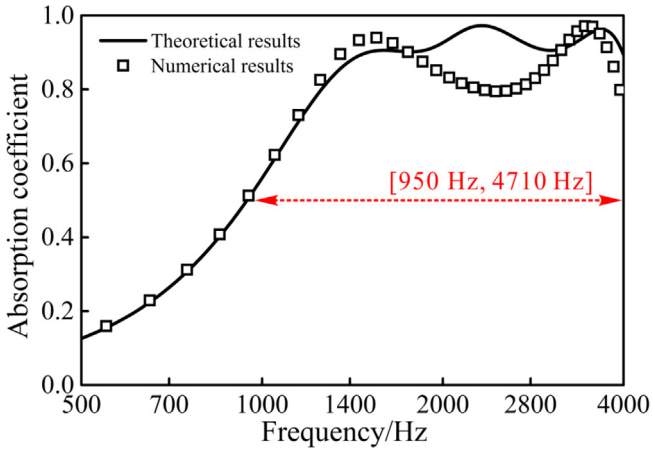

Fig. 13. Sound absorption coefficient of optimized PHCH at 700 K.

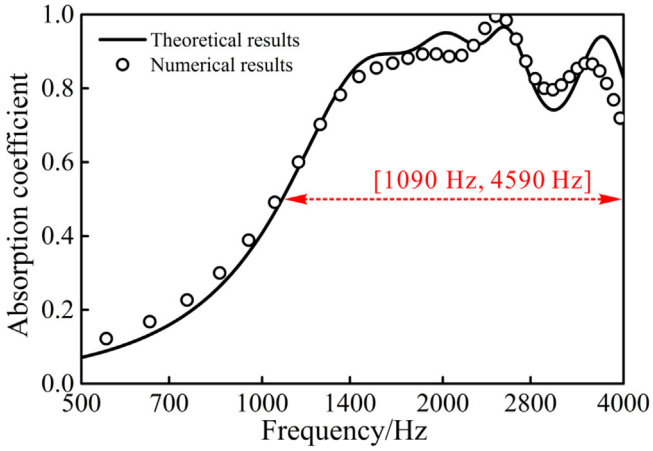

Fig. 14. Sound absorption coefficient of optimized HCH at 700 K.

half-absorption bands of PHCH, HCH and PH are 950 Hz, 1090 Hz and 990 Hz, respectively. On the other hand, the half-absorption bandwidths of PHCH, HCH and PH are 2.310 octaves, 2.074 octaves and 1.985 octaves, respectively. The optimization process has maintained the independence of each structure, with only the total thickness being the same. So on this condition, PHCH has demonstrated its advantages in low-frequency absorption potential over its competitors. Because the present absorption curves are obtained via optimization from 500 Hz to 4000 Hz, the comparison of average sound absorption is significative. The theoretical/numerical average sound absorption coefficients of PHCH, HCH and PH are 0.82/0.78, 0.76/0.75 and 0.71/0.69,

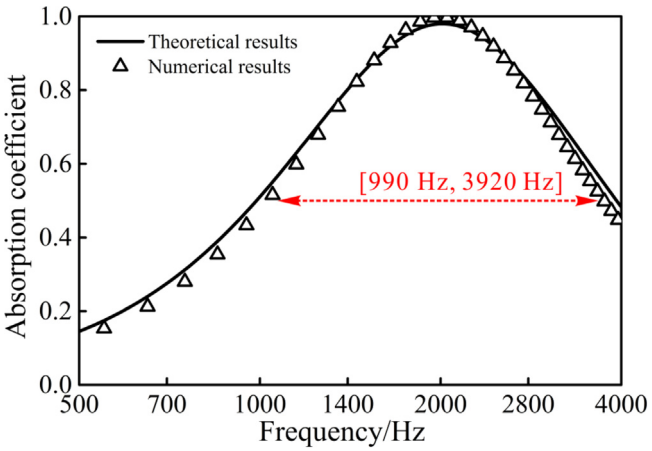

Fig. 15. Sound absorption coefficient of optimized PH at 700 K.

respectively. Thus, in terms of averaged performance, PHCH still behaves the best.

4.4. Influences of the facesheet and the corrugation

The facesheet has more significance than the corrugation in influencing the sound absorption performance at room temperature [49], although the latter one is also an indispensable component of PHCH. Taking the temperature into account, the average sound absorption coefficients changing with the facesheet thickness and the corrugation thickness are presented in Fig. 16 for PHCH-cored sandwich panels. Other parameters not discussed are identical as Sample A in Table 2. Within the same variation range and under the same temperature scale, the average absorption coefficient shows a wider scope with the change of facesheet thickness than that of corrugation thickness. So in a larger scale of temperature, the results of Fig. 16 suggest that the facesheet still plays a more important role than the corrugation.

In Fig. 16, the blue arrows reveal the variation tendency of the average absorption coefficient. The arrow in the Fig. 16(a) becomes smaller from the upper left to the lower right, while the arrow in Fig. 16(b) gets bigger first and then turns smaller from the lower left to the upper right, divided by a dashed boundary line. First, the average absorption coefficient increases with increasing temperature in Fig. 16(a), showing the same trend with the area on the left of the boundary line in Fig. 16(b). This means that, when the corrugation is of sub-millimeter scale, the average absorption performance is enhanced as temperature is increased, consistent with the variation trend revealed in Fig. 5. Second, the results of Fig. 16 demonstrate that good absorption performance requires sub-millimeter thicknesses of both the facesheet and the corrugation. While it would be better for the facesheet to be as thin as possible, the corrugation is required to be 0.5 mm to 1 mm.

5. Conclusions

The ability of micro-perforated sandwich panel with perforated honeycomb- corrugation hybrid core (PHCH) at high temperatures is studied both theoretically and numerically, and compared with micro-perforated sandwich panels with honeycomb-corrugation hybrid core (HCH) and honeycomb core (PH). Built upon the acoustic impedance theory and the electro-acoustic analogy method, the surface impedance and the sound absorption coefficient of the proposed structure are calculated with consideration of temperature variation, as well as dynamic viscosity and viscous boundary layer thickness. Acoustical properties including sound absorption, surface impedance and particle velocity are obtained theoretically and/or numerically to explore the sound absorption of PHCH-, HCH- and PH-cored sandwich panels. Optimizations are subsequently performed to further verify the advantages of PHCH in low-frequency absorption and broadband absorption potential over its competitors. The theoretical model is also employed to quantify the influences of facesheet and corrugation thicknesses on average absorption coefficient over a wide range of temperatures. Main findings are summarized as follows:

(1) As the temperature rises, both the dynamic viscosity and viscous boundary layer thickness increase, resulting in strengthened viscous effects.
(2) The sound absorption curve and its peak move to higher frequencies as the temperature is increased. Meanwhile, the specific impedance curve becomes flat. The real part of the specific impedance curve moves upward as a whole, while the imaginary part moves downward.
(3) Air particles in the perforations vibrate most severely when the sound absorption curve reaches its peak, which is also the critical time when resonance occurs.
(4) At high temperatures, PHCH behaves best at low frequencies and possesses the broadest bandwidth compared to HCH and PH, because its half-absorption bandwidth starts at the lowest frequency and ends at the highest frequency, if the total thickness of the structure is kept unchanged.
(5) The facesheet has more influence on sound absorption than the corrugation over the entire temperature range considered.

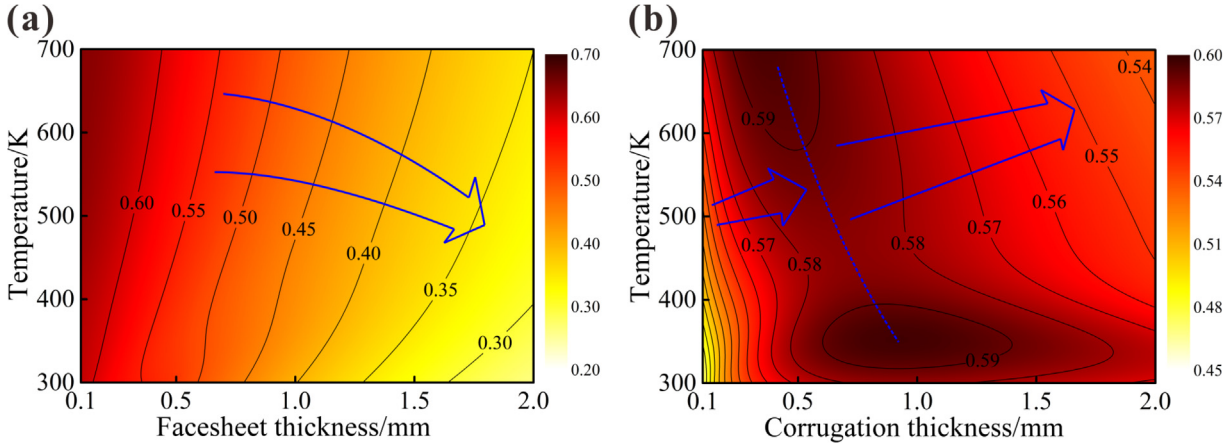

Fig. 16. Average sound absorption coefficient of PHCH-cored sandwich panel from 500 Hz to 4000 Hz at different temperatures: (a) changing with facesheet thickness; (b) changing with corrugation thickness.

Acknowledgements

This work was supported by NSFC (11761131003, U1737107 and 11772248), DFG (ZH15/32-1) and the Fundamental Research Funds for the Central Universities (Z201811253).

References

[1] Cao J, Grenestedt JL. Design and testing of joints for composite sandwich/steel hybrid ship hulls. Compos Part A-Appl S 2004;35(9):1091–105.
[2] Mäkinen KE, Hellbratt SE, Olsson KA. The development of sandwich structures for naval vessels during 25 years. Springer; 1998.
[3] Zimmerman S. Submarine technology for the 21st century. Pasha Publications Inc; 1997.
[4] Burcher R, Rydill L. Concepts in submarine design. Cambridge University; 1994.
[5] Kim YH, Han JW, Kim DW, et al. A study for the characteristic changes under the repeated thermal exposure in the process of repairing aircraft sandwich structures. Int J Mod Phys B 2003;17:1839.
[6] Zumpano G, Meo M. Damage detection in an aircraft foam sandwich panel using nonlinear elastic wave spectroscopy. Comput Struct 2008;86(3):483–90.
[7] Lee BJ, Pessiki S. Thermal performance evaluation of precast concrete three-wythe sandwich wall panels. Energy Buildings 2006;38(8):1006–14.
[8] Kawasaki T, Kawai S. Thermal insulation properties of wood-based sandwich panel for use as structural insulated walls and floors. J Wood Sci 2006;52(1):75–83.
[9] Zhou R, Crocker MJ. Sound transmission loss of foam-filled honeycomb sandwich panels using statistical energy analysis and theoretical and measured dynamic properties. J Sound Vib 2010;329(6):673–86.
[10] Endo M, Kim YS. Study on direct sound reduction structure for reducing noise generated by vibrating solids. J Sound Vib 2013;332(11):2643–58.
[11] Talebitooti R, Choudari Khameneh A, Zarastvand M, et al. Investigation of three-dimensional theory on sound transmission through compressed poroelastic sandwich cylindrical shell in various boundary configurations. J Sandw Struct Mater 2018;109963621775156.
[12] Talebitooti R, Gohari HD, Zarastvand MR. Multi objective optimization of sound transmission across laminated composite cylindrical shell lined with porous core investigating Non-dominated Sorting Genetic Algorithm. Aerosp Sci Technol 2017;69:269–80.
[13] Talebitooti R, Zarastvand MR. The effect of nature of porous material on diffuse field acoustic transmission of the sandwich aerospace composite doubly curved shell. Aerosp Sci Technol 2018;78:157–70.
[14] Talebitooti R, Zarastvand MR, Gohari HD. The influence of boundaries on sound insulation of the multilayered aerospace poroelastic composite structure. Aerosp Sci Technol 2018;80:452–71.
[15] Xin FX, Lu TJ. Transmission loss of orthogonally rib-stiffened double-panel structures with cavity absorption. J Acoust Soc Am 2011;129(4):1919–34.
[16] Xin FX, Lu TJ. Sound radiation of orthogonally rib-stiffened sandwich structures with cavity absorption. Compos Sci Technol 2010;70(15):2198–206.
[17] Xin FX, Lu TJ. Analytical modeling of fluid loaded orthogonally rib-stiffened sandwich structures: sound transmission. J Mech Phys Solids 2010;58(9):1374–96.
[18] Asdrubali F, Pispola G. Properties of transparent sound-absorbing panels for use in noise barriers. J Acoust Soc Am 2007;121(1):214–21.
[19] Yang C, Cheng L. Sound absorption of microperforated panels inside compact acoustic enclosures. J Sound Vib 2016;360:140–55.
[20] Toyoda M, Sakagami K, Takahashi D, et al. Effect of a honeycomb on the sound absorption characteristics of panel-type absorbers. Appl Acoust 2011;72(12):943–8.
[21] Gerald WB, John WP, Alan SH. Advanced turbofan duct liner concepts. Langley Research Center; 1999.
[22] Sakagami K, Nakajima K, Morimoto M, et al. Sound absorption characteristics of a honeycomb-backed microperforated panel (MPP) absorber. J Acoust Soc Am 2006;120(5):3146.
[23] Lin JH, Lin CM, Huang CC, et al. Evaluation of the manufacture of sound absorbent sandwich plank made of PET/TPU honeycomb grid/PU foam. J Compos Mater 2011;45(13):1355–62.
[24] Ruiz H, Cobo P. Sound absorption of single- and double-layer microperforated insertion units. J Acoust Soc Am 2010;128(4):2286.
[25] Wei K, Peng Y, Qu Z, et al. High temperature mechanical behaviors of lightweight ceramic corrugated core sandwich panel. Compos Struct 2017;176:379–87.
[26] Wei K, Peng Y, Wang K, et al. High temperature mechanical properties of lightweight C/SiC composite pyramidal lattice core sandwich panel. Compos Struct 2017;178:467–75.
[27] Shen HS, Li SR. Postbuckling of sandwich plates with FGM face sheets and temperature-dependent properties. Compos Part B-Eng 2008;39(2):332–44.
[28] Vangipuram P, Ganesan N. Buckling and vibration of rectangular composite viscoelastic sandwich plates under thermal loads. Compos Struct 2007;77(4):419–29.
[29] Frostig Y, Thomsen OT. On the free vibration of sandwich panels with a transversely flexible and temperature dependent core material – part II: numerical study. Compos Sci Technol 2009;69(6):863–9.
[30] Xia XK, Shen HS. Vibration of post-buckled sandwich plates with FGM face sheets in a thermal environment. J Sound Vib 2008;314(1–2):254–74.
[31] Wang ZX, Shen HS. Nonlinear vibration and bending of sandwich plates with nanotube-reinforced composite face sheets. Compos Part B-Eng 2012;43(2):411–21.
[32] Jen YM, Lin HB. Temperature-dependent monotonic and fatigue bending strengths of adhesively bonded aluminum honeycomb sandwich beams. Mater Des 2013;45:393–406.
[33] Assaf S, Guerich M. Influence of temperature on sound transmission through viscoelastic sandwich plates. J Acoust Soc Am 2008;123(5):3729.
[34] Sun F, Chen H, Wu J, et al. Sound absorbing characteristics of fibrous metal materials at high temperatures. Appl Acoust 2010;71(3):221–35.
[35] Giese F, Ries HC, Eigenbrod C. On the performance of porous sound absorbent material in high temperature applications. J Eng Gas Turb Power 2010;132(12):1113–22.
[36] Christie DRA. Measurement of the acoustic properties of a sound absorbing material at high temperatures. J Sound Vib 1976;46(3):347–55.
[37] Najib NN, Ariff ZM, Bakar AA, et al. Correlation between the acoustic and dynamic mechanical properties of natural rubber foam: effect of foaming temperature. Mater Des 2011;32(2):505–11.
[38] Liu XY, Zhan MS, Wang K. Influence of foam structure and service environment on sound absorption characteristics of polyimide foams. High Perform Polym 2012;24(7):646–53.
[39] Han B, Qin K, Yu B, et al. Honeycomb-corrugation hybrid as a novel sandwich core for significantly enhanced compressive performance. Mater Des 2015;93:271–82.
[40] Han B, Wang W, Zhang Z, et al. Performance enhancement of sandwich panels with honeycomb–corrugation hybrid core. Theor Appl Mech Lett 2016;6(1):54–9.
[41] Tang Y, Ren S, Meng H, et al. Hybrid acoustic metamaterial as super absorber for broadband low-frequency sound. Sci Rep 2017;7:43340.
[42] Delany M, Bazley E. Acoustical properties of fibrous absorbent materials. Appl Acoust 1970;3(2):105–16.
[43] Verdière K, Panneton R, Elkoun S, et al. Transfer matrix method applied to the parallel assembly of sound absorbing materials. J Acoust Soc Am 2013;134(6):4648–58.
[44] Brekhovskikh L. Waves in Layered Media Vol. 16. Elsevier; 2012.
[45] Crandall IB. Theory of vibrating systems and sound. Van Nostrand; 1926.
[46] Maa DY. Theory and design of microperforated panel sound-absorbing constructions. Sci Sinica 1975;18(1):55–71.
[47] Smits AJ, Dussauge JP. Turbulent shear layers in supersonic flow. 2nd ed. Springer; 2006.
[48] Williams F, John E. Sound and sources of sound. Ellis Horwood; 1983.
[49] Tang Y, Li F, Xin F, et al. Heterogeneously perforated honeycomb-corrugation hybrid sandwich panel as sound absorber. Mater Des 2017;134:502–12.